Rhodococcus l -Phenylalanine Dehydrogenase: Kinetics, Mechanism, and Structural Basis for Catalytic Specifity † , ‡

ARTICLE *in* BIOCHEMISTRY · SEPTEMBER 2000

Impact Factor: 3.02 · DOI: 10.1021/bi000494c · Source: PubMed

4 AUTHORS, INCLUDING:

James B Thoden
University of Wisconsin–Madison
131 PUBLICATIONS **5,161** CITATIONS

SEE PROFILE

Rhodococcus L-Phenylalanine Dehydrogenase: Kinetics, Mechanism, and Structural Basis for Catalytic Specificity[†,‡]

Norbert M. W. Brunhuber,[||,#] James B. Thoden,[§] John S. Blanchard,*[,||] and Janeen L. Vanhooke*[,⊥]

Department of Biochemistry, Albert Einstein College of Medicine, 1300 Morris Park Avenue, Bronx, New York 10461, and Department of Biochemistry and Institute for Enzyme Research, University of Wisconsin−Madison, Madison, Wisconsin 53706

Received March 3, 2000; Revised Manuscript Received May 25, 2000

ABSTRACT: Phenylalanine dehydrogenase catalyzes the reversible, pyridine nucleotide-dependent oxidative deamination of L-phenylalanine to form phenylpyruvate and ammonia. We have characterized the steady-state kinetic behavior of the enzyme from *Rhodococcus* sp. M4 and determined the X-ray crystal structures of the recombinant enzyme in the complexes, E·NADH·L-phenylalanine and E·NAD^+·L-3-phenyllactate, to 1.25 and 1.4 Å resolution, respectively. Initial velocity, product inhibition, and dead-end inhibition studies indicate the kinetic mechanism is ordered, with NAD^+ binding prior to phenylalanine and the products' being released in the order of ammonia, phenylpyruvate, and NADH. The enzyme shows no activity with NADPH or other 2′-phosphorylated pyridine nucleotides but has broad activity with NADH analogues. Our initial structural analyses of the E·NAD^+·phenylpyruvate and E·NAD^+·3-phenylpropionate complexes established that Lys78 and Asp118 function as the catalytic residues in the active site [Vanhooke et al. (1999) *Biochemistry 38,* 2326−2339]. We have studied the ionization behavior of these residues in steady-state turnover and use these findings in conjunction with the structural data described both here and in our first report to modify our previously proposed mechanism for the enzymatic reaction. The structural characterizations also illuminate the mechanism of the redox specificity that precludes α-amino acid dehydrogenases from functioning as α-hydroxy acid dehydrogenases.

Phenylalanine dehydrogenase (L-phenylalanine:NAD^+ oxidoreductase, deaminating; EC 1.4.1.20) catalyzes the reversible pyridine nucleotide-dependent oxidative deamination of L-phenylalanine:

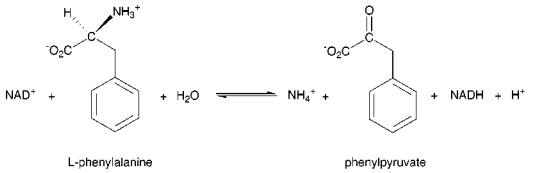

The enzyme was first isolated from a *Brevibacterium* species (*1*) and has since been identified from several other bacterial sources, including *Bacillus* and *Sporosarcina* (*2*), *Nocardia* (*3*), and *Thermoactinomyces* (*4*). A particularly stable phenylalanine dehydrogenase was identified by Hummel and coworkers in *Rhodococcus* sp. M4 (*5*), a soil bacterium that expresses the enzyme at high levels when grown in the presence of L-phenylalanine. The *Rhodococcus* phenylalanine dehydrogenase has limited substrate activity with phenylpyruvate analogues, although phenylketobutyrate is a reasonably good substrate for the enzyme. Enzyme-catalyzed reductive amination of phenylketobutyrate is potentially useful for the production of optically pure L-homophenylalanine, a component of an angiotensin converting enzyme (ACE) inhibitor used in the treatment of hypertension and heart failure (*6, 7*). The enzyme is also being developed as a biosensor to screen for phenylketonuria (*8, 9*) and has industrial uses for the production of optically pure L-phenylalanine (*10*), a component of the artificial sweetener aspartame.

We recently reported the molecular structures of the recombinant *Rhodococcus* sp. M4 phenylalanine dehydrogenase in the inhibitory ternary complexes, E·NAD^+·phenylpyruvate and E·NAD^+·3-phenylpropionate (*11*). The enzyme crystallizes as a homodimer, with approximate overall dimensions of 82 Å × 75 Å × 75 Å. Each monomeric subunit is composed of large N- and C-terminal domains that are separated by a deep cleft containing the active site. The C-terminal domain contains a "Rossman" fold (*12*) and provides binding interactions for the pyridine nucleotide. The N-terminal domain binds the amino acid and is similar to the amino acid binding domains of other amino acid dehydrogenases of known structure (*13*−*15*). The two active sites of the dimer are separated by a distance of ap-

[†] This work was supported by the National Institutes of Health Grants GM 33449 (to J.S.B.) and DK47814 (to Dr. Hazel M. Holden) and the National Institutes of General Medical Sciences Training Program in Pharmacological Sciences Grant 5T32 GM 07260. Some of the material in this paper is from a thesis submitted in partial fulfillment of the requirements for the degree of Doctor of Philosophy in the Sue Golding Graduate Division of Medical Sciences, Albert Einstein College of Medicine.

[‡] X-ray coordinates have been deposited in the RCSB Protein Data Band (1C1D and 1C1X) and will be released upon publication.

* Address correspondence concerning the enzymology to J.S.B. Phone: (718) 430-3096. Fax: (718) 430-8565. Address correspondence concerning the crystallography to J.L.V. at the Department of Biochemistry, University of Wisconsin−Madison, 433 Babcock Dr., Madison, WI 53706.

[||] Albert Einstein College of Medicine.

[§] Institute for Enzyme Research, University of Wisconsin−Madison.

[⊥] Department of Biochemistry, University of Wisconsin−Madison.

[#] Present address: Medical Action Communications, 20 Commerce Dr., Cranford, NJ 07016.

10.1021/bi000494c CCC: $19.00
Published on Web 07/11/2000

proximately 50 Å. The interactions that constitute the subunit interface within the dimer are contributed primarily by β-strand A (residues Met12 to Asp18) of each monomer. These β-strands run antiparallel, and their interaction connects the five-stranded N-terminal β-sheets of the two subunits.

These structures revealed significantly different binding modes for 3-phenylpropionate and phenylpyruvate in the active site of the enzyme. 3-Phenylpropionate is positioned with its Cα at a distance of 4.2 Å from the C4 of the nicotinamide, and direct hydride transfer to the nicotinamide is easily envisioned. As such, the orientation of this ligand mimics the orientation expected for L-phenylalanine. The corresponding distance between the Cα of phenylpyruvate and the nicotinamide is greater than 6 Å, a consequence of the hydrogen bonds formed by the keto oxygen of phenylpyruvate with Lys78 and Gly40. These hydrogen bonds effectively remove the α-keto acid from the dinucleotide, preventing the direct reduction of this ligand to generate the α-hydroxy acid product.

The goals of our investigation of phenylalanine dehydrogenase are to explain the chemical mechanism and establish the basis of the specificity for the reaction catalyzed by this, and other, enzymes of the amino acid dehydrogenase family. To this end, we have characterized the kinetic behavior of the enzyme and determined the three-dimensional structures of two additional species, namely the E·NADH·L-phenylalanine and E·NAD^+·L-3-phenyllactate ternary complexes. This analysis has prompted a revision of our previously proposed chemical mechanism for the enzymatic reaction (*11*) and firmly establishes the nature of the discrimination between α-amino acids and α-hydroxy acids as substrates for oxidation by amino acid dehydrogenases.

EXPERIMENTAL PROCEDURES

Materials. Rhodococcus sp. M4 was the generous gift of Dr. Werner Hummel (Institut für Enzymtechnologie, Jülich, Germany) and was maintained on plates containing 1% yeast extract (Difco), 1% L-phenylalanine, 0.4% K_2HPO_4, and 18 g/L of agar (Difco) at pH 7.5. For liquid cultures, the media contained 2% yeast extract, 1.5% L-phenylalanine, 1% glycerol, and 1% K_2HPO_4, at pH 7.5. Chemicals, buffers, substrates, substrate analogues, dinucleotide substrates and analogues, D-glucose-1-*d* (97 atom % D), *Leuconostoc mesenteroides* glucose-6-phosphate dehydrogenase, *Streptococcus faecalis* NADH peroxidase, and Baker's yeast hexokinase were purchased from Sigma. Protease inhibitors and streptomycin sulfate were purchased from Boehringer Mannheim. [2-^{2}H]-L-Phenylalanine (96 atom % D) was purchased from Cambridge Isotope Labs.

Bacterial Growth. A single colony from an agar plate was cultured in liquid medium at 30 °C for approximately 48 h. This starter culture was used to inoculate 500 mL of fresh medium, and this culture was subsequently used to inoculate 6 L of medium in 2-L baffled culture flasks (1 L/flask). The cells reached late log phase in approximately 20 h, at which time they were collected by centrifugation, weighed, resuspended in buffer, and stored at −70 °C. Both the pH and the level of L-phenylalanine were monitored during the growth, and sterile 1% K_2HPO_4 and solid L-phenylalanine were added to maintain the pH and to keep the concentration of amino acid as high as possible (ca. 1 mM).

Enzyme Purification. All procedures were performed at 4 °C. Frozen cells were thawed and protease inhibitors were added directly to the suspension of cells (typically, 2.3 mg/L leupeptin, 52 mg/L TLCK,[1] 20 mg/L soybean trypsin inhibitor, 1.6 mg/L aprotinin, 1.1 mg/L pepstatin, and 36 mg/L PMSF). An equal volume of acid-washed glass beads (<106 μm, Sigma) was added to the suspension, and the cells were broken in a Bead-beater apparatus (Bio-spec Products). The cell debris and glass beads were pelleted by centrifugation at 12 000 rpm for 45 min. Nucleic acids were precipitated from the supernatant by the addition of streptomycin sulfate (1% final concentration). The resulting suspension was centrifuged for 45 min at 12 000 rpm to pellet the nucleic acids.

The nucleic acid-free supernatant was dialyzed against 25 mM TEA (pH 7.8) containing 50 mM NaCl (buffer A). A precipitate formed during dialysis and was removed by ultracentrifugation. The clarified extract was loaded onto a 5- × 35-cm column of Q Sepharose Fast Flow (Pharmacia) and was then eluted by using a 2-L gradient of NaCl that increased nonlinearly from 0.05 to 1.0 M. Phenylalanine dehydrogenase activity emerged between 0.65 and 0.80 M NaCl, and the active fractions were pooled and dialyzed against 50 mM TEA (pH 7.8) containing 50 mM NaCl (buffer B). This solution was loaded onto a 100-mL Red A dye column (Amicon), which was subsequently washed with buffer B until A_{280} decreased to below 0.1. Phenylalanine dehydrogenase was eluted from the column by using 50 mM TEA (pH 7.8) containing 1 M NaCl. Active fractions were pooled, dialyzed against buffer B, and then applied to a 1- × 10-cm Mono Q anion-exchange column (Pharmacia) that had been preequilibrated in buffer B. The enzyme emerged from the column between 0.45 and 0.55 M NaCl using a 100-mL nonlinearly increasing gradient of NaCl (0.05−1.0 M). Active fractions were pooled and stored either as a 50% glycerol solution or as an ammonium sulfate precipitate (2.4 M final concentration). The enzyme retained activity for greater than 6 months at 4 °C.

Analytical Methods. The isoelectric point of phenylalanine dehydrogenase was determined by isoelectric focusing on a polyacrylamide gel containing ampholytes (Phastsystem, Pharmacia). The subunit molecular mass was estimated by SDS−PAGE. The apparent native molecular mass was determined by size-exclusion chromatography on a Superdex 200 column (Pharmacia) with molecular mass standards (Bio-Rad). The absorbance at 280 nm of a 1.0 mg/mL solution of phenylalanine dehydrogenase in a buffer of 25 mM TEA (pH 7.8) containing 400 mM NaCl was determined in a Gilford 260 spectrophotometer.

Enzyme Assay. The reaction rates of *Rhodococcus* sp. M4 phenylalanine dehydrogenase were monitored spectrophotometrically with a Gilford 260 spectrophotometer maintained

[1] Abbreviations: CAPS, 3-(cyclohexylamino)-1-propanesulfonic acid; CHES, 2-(*N*-cyclohexylamino)ethanesulfonic acid; DEAE, diethylaminoethyl; EDTA, ethylenediaminetetraacetic acid; EPPS, *N*-(2-hydroxyethyl)piperazine-*N*′-3-propanesulfonic acid; FPLC, fast protein liquid chromatography; NHD^+, oxidized β-nicotinamide hypoxanthine dinucleotide; $NHDP^+$, oxidized β-nicotinamide hypoxanthine dinucleotide phosphate; NGD^+, oxidized β-nicotinamide guanine dinucleotide; PMSF, phenylmethyl sulfonyl fluoride; SDS−PAGE, sodium dodecyl sulfate polyacrylamide gel electrophoresis; TEA, triethanolamine; TLCK, L-1-chlor-3-(4-tosylamido)-7-amino-2-heptanon-hydrochloride.

at 25 °C by a circulating water bath and thermospacers. Absorbance changes were recorded on a 10-mV strip chart recorder. pH measurements were determined directly in the cuvette using a Radiometer PHM62 pH meter equipped with a combined microelectrode. Reactions were initiated by the addition of a small volume (25 μL) of cold enzyme to a temperature-equilibrated solution containing various concentrations of substrates.

Equilibrium Constant Determination. Three cuvettes containing 1.0 mM NAD^+ and 1.0 mM L-phenylalanine in 100 mM EPPS buffer (pH 8.01) were prepared and monitored for the production of NADH at 340 nm and 25 °C after the addition of enzyme. Once equilibrium had been reached, the final absorbance at 340 nm was recorded, the pH was measured, and the equilibrium constant was calculated using eq 1, where millimolar concentrations of the products, NADH, phenylpyruvate, and NH_4^+, were determined using $\epsilon_{340} = 6.22$ mM^{-1} cm^{-1}.

$$K_{eq}' = [\text{NADH}][\text{phenylpyruvate}][NH_4^+]/[NAD^+][\text{L-phenylalanine}] \quad (1)$$

Alternate Nucleotide Substrates. The kinetic parameters exhibited by alternate nucleotide substrates were determined at saturating levels of L-phenylalanine (55 mM). Oxidized nucleotide solutions were calibrated enzymatically with *L. mesenteroides* glucose-6-phosphate dehydrogenase and excess glucose-6-phosphate. All assays were performed in 100 mM CAPS buffer (pH 10.0), and the reaction rates were monitored at the indicated wavelengths using the indicated molar extinction coefficients. NADH, NHDH, NGDH, NADPH, 2′,3′-cyclic-NADPH, and NHDPH, $\epsilon_{340} = 6220$ M^{-1} cm^{-1}; thioNAD(P)H, $\epsilon_{395} = 11\,300$ M^{-1} cm^{-1}; 3-pyridinealdehyde-NADH, $\epsilon_{358} = 9300$ M^{-1} cm^{-1}; and 3-acetylpyridine-NAD(P)H, $\epsilon_{363} = 9100$ M^{-1} cm^{-1}.

Stereochemistry of Hydride Transfer. NADH and [4*S*-^{2}H]-NADH were prepared from NAD^+ in 100 mM ammonium bicarbonate (pH 8.0), using yeast hexokinase, *L. mesenteroides* glucose-6-phosphate dehydrogenase, and an excess of ATP, $MgCl_2$, and either glucose or glucose-1-*d*, respectively. The reduced nucleotides were purified on a 1- × 10-cm Mono Q anion-exchange column using a gradient of ammonium bicarbonate that increased nonlinearly from 0.01 to 1.0 M (*16*). The reduced nucleotides eluted from the column at approximately 180 mM ammonium bicarbonate. The NADH and [4*S*-^{2}H]NADH solutions were each made 1.0 mM in phenylpyruvate, after which phenylalanine dehydrogenase was added, and the reaction was monitored spectrophotometrically until complete. Each sample was concentrated by rotary evaporation to remove excess ammonium bicarbonate. The samples were analyzed by mass spectrometry at the Albert Einstein College of Medicine Laboratory for Macromolecular Analysis using FAB-MS and a Finnigan MAT.

Initial Velocity, Product, and Dead-End Inhibition Studies. All kinetic mechanism studies were performed in 100 mM CHES buffer (pH 9.2). NAD^+ solutions were calibrated enzymatically by using an excess of glucose-6-phosphate and glucose-6-phosphate dehydrogenase, and NADH solutions were calibrated by using *S. faecalis* NADH peroxidase and an excess of hydrogen peroxide. Phenylpyruvate solutions were calibrated using phenylalanine dehydrogenase and an excess of NADH and NH_4^+. Finally, L-phenylalanine solutions were calibrated spectrophotometrically using an extinction coefficient of 151.5 M^{-1} cm^{-1} (*17*) at 263.7 nm in 100 mM phosphate buffer (pH 7.1).

Steady-State Kinetic Analysis. Reciprocal initial velocities were plotted against the reciprocal of the variable substrate concentration, and the data were fitted to the appropriate rate equations by the weighted least-squares method, assuming equal variances of the velocity. The Fortran fitting programs of Cleland (*18*) were modified to run on a personal computer. Intersecting initial velocity patterns were fitted to eq 2, while parallel initial velocity patterns were fitted to eq 3. Competitive, uncompetitive, and noncompetitive inhibition were fitted to eqs 4, 5, and 6, respectively. Double-reciprocal plots used to obtain kinetic parameters of alternate nucleotides were fit to eq 7.

$$v = V_{max}AB/[K_aB + K_bA + AB + K_{ia}K_b] \quad (2)$$

$$v = V_{max}AB/[K_aB + K_bA + AB] \quad (3)$$

$$v = V_{max}A/[(K_m(1 + I/K_{is}) + A] \quad (4)$$

$$v = V_{max}A/[K_m + A(1 + I/K_{ii})] \quad (5)$$

$$v = V_{max}A/[K_m(1 + I/K_{is}) + A(1 + I/K_{ii})] \quad (6)$$

$$v = V_{max}A/[K_m + A] \quad (7)$$

pH Dependence of the Phenylalanine Dehydrogenase Reaction. The kinetic constants *V* and *V*/*K* were determined at various pH values for each substrate by varying the concentration of that substrate at saturating concentrations of all other substrates. When phenylpyruvate was used as the variable substrate, NADH was present at a saturating concentration, and NH_4^+ was held at either saturating or 0.1 K_m (5 mM) concentration. Reactions were performed at overlapping pH values to eliminate specific buffer effects.

Data Analysis of pH Profiles. The p*K* values of groups whose ionizations affect the kinetic parameters were obtained by fitting the pH profiles to eqs 8−11. These equations describe curves that decrease with a unit slope below pK_1 and above pK_2 (eq 8), decrease with unit slope below pK_1 and then decrease with a slope of 2 below pK_2 (eq 9), decrease with a unit slope above pK_1 (eq 10), or decrease with a unit slope below pK_1 and above pK_2, and decrease with a slope of 2 below a p*K* of (pK_0 − pK_1) (eq 11). In these equations, *H* represents the H^+ concentration, and *C* is the pH-independent value of *Y*, the kinetic parameter whose pH-dependent behavior is being investigated, at the optimal state of protonation.

$$\log Y = \log[C/(1 + H/K_1 + K_2/H)] \quad (8)$$

$$\log Y = \log[C/(1 + H/K_1 + H^2/K_1K_2)] \quad (9)$$

$$\log Y = \log[C/(1 + K_1/H] \quad (10)$$

$$\log Y = \log[C/(1 + H^2/K_0 + H/K_1 + K_2/H)] \quad (11)$$

The pH dependence of the pK_i of the competitive, dead-end inhibitor 3-phenylpropionate was determined by measuring

Table 1: Intensity Statistics

E•NADH•L-phenylalanine complex											
	resolution range (Å)										
	overall	50−2.69	2.14	1.87	1.70	1.57	1.48	1.41	1.35	1.29	1.25
observations	1286363	125627	152076	149601	143046	137449	130721	121972	114047	107971	103853
independent reflections	216285	20318	22443	22328	22124	21994	21873	21693	21567	21435	20510
completeness (%)	96.5	87.6	99.4	99.4	99.0	98.6	98.1	97.7	97.1	96.5	92.1
avg I/avg $\sigma(I)$	24.4	26.5	34.8	33.6	26.2	18.9	13.4	8.7	6.0	4.6	3.4
$R_{\text{factor (\%)}}$[a]	6.1	5.2	5.3	5.7	6.9	8.7	10.8	14.5	18.5	21.9	25.5
E·NAD$^+$·L-3phenyllactate complex											
	resolution range (Å)										
	overall	50−3.02	2.39	2.09	1.90	1.76	1.66	1.58	1.51	1.45	1.40
observations	735380	79016	90318	88323	86254	77804	72876	68373	63667	57835	50914
independent reflections	156183	15377	16099	15938	15935	15761	15628	15542	15476	15370	15057
completeness (%)	97.0	91.8	99.2	98.9	99.1	98.2	97.8	97.3	96.9	96.3	94.7
avg I/avg $\sigma(I)$	22.1	24.8	31.8	30.0	25.3	16.8	11.1	8.0	5.8	4.2	3.0
$R_{\text{factor (\%)}}$[a]	5.3	3.9	4.6	5.4	6.6	8.5	11.5	14.5	17.7	22.2	27.1

[a] $R_{\text{factor}} = (\Sigma|I - \bar{I}|/\Sigma I) \times 100$.

its K_i value versus L-phenylalanine as a function of pH. The K_i values were obtained by fitting the data at any pH value to eq 4. The pK value for the group whose ionization influenced phenylpropionate binding was determined by fitting the reciprocal of the K_i value to eq 10.

Structural Determination of the E·NADH·L-phenylalanine Complex. Recombinant L-phenylalanine dehydrogenase was purified from *E. coli* BL21 (DE3) cells carrying the overexpression plasmid pBL-1B, as previously described (*11*). Crystals of the E·NADH·L-phenylalanine complex were grown at room temperature by macroseeding small crystals into 20-μL batch setups on Plexiglas depression plates. The batch solution was prepared by quickly mixing a 7.5 mg/mL solution of enzyme, buffered in 50 mM triethanolamine (pH 7.8), containing 100 mM NaCl, 10 mM NADH, and 20 mM L-phenylalanine with an equal volume of precipitant solution composed of 2.55 M Na^+/K^+ phosphate, 100 mM CHES (pH 8.7), and 4% (v/v) 2-propanol. The crystals grew as rectangular, bladed tablets and achieved typical dimensions of 0.6 mm × 0.3 mm × 0.2 mm within 6 days. They belonged to the orthorhombic space group $P2_12_12_1$, with unit cell dimensions of $a = 64.8$ Å, $b = 110.6$ Å, and $c = 113.3$ Å and with a dimer in the asymmetric unit.

Prior to X-ray data collection, the crystals were equilibrated overnight in a synthetic mother liquor composed of 1.6 M Na^+/K^+ phosphate, 50 mM CHES (pH 8.7), 2% (v/v) 2-propanol, 10 mM NADH, and 20 mM L-phenylalanine. The following day the crystals were rapidly transferred in a stepwise fashion to a cryoprotectant solution containing 1.9 M Na^+/K^+ phosphate, 50 mM CHES (pH 8.7), 2% (v/v) 2-propanol, 10 mM NADH, 20 mM L-phenylalanine, and 10% (v/v) ethylene glycol. The crystals were suspended in a loop of 20 μm surgical thread, flash-cooled to −160 °C in a stream of nitrogen gas, and stored in liquid nitrogen until data collection.

X-ray data to 1.25-Å resolution were collected from a single crystal at the Structural Biology Center Beamline 19-ID located at the Advanced Photon Source. The crystal was exposed to radiation of wavelength 0.7433 Å, and the X-ray reflections were recorded on the SBC APS2 3 × 3 CCD array detector, which was positioned at a distance of 155 mm from the crystal. A total of 700 frames was collected while using a per-frame oscillation angle of 0.25° and an exposure time of 2.5 s.

The frames were processed by using the program DENZO and scaled using SCALEPACK (*19*). From the 700 frames, 1 286 363 reflections were integrated, which reduced to 216 285 unique reflections after scaling. Relevant X-ray data-collection statistics for this data set are given in Table 1.

The structure of the E·NADH·L-phenylalanine complex was solved by difference Fourier techniques, with the protein coordinates of the E·NAD$^+$·phenylpyruvate complex serving as the initial model. After several cycles of refinement by using the program TNT (*20*), solvent molecules, the dinucleotide, and L-phenylalanine were positioned into the electron density map by using the software program FRODO (*21*). Alternate cycles of least-squares refinement using TNT and model building using the software program TURBO-FRODO (*22*) were subsequently performed to refine the model of the complex.

The electron density map was very well-defined. The following amino acid residues were modeled into the density in alternate conformations: Ser4, Met74, Ser123, Glu247, and Glu347 in subunit I, and Asp55, Met74, Ser110, Ser123, Leu170, Asp174, Ser192, Ser255, and Ser271 in subunit II. The average B-values for all main-chain backbone atoms were 15.81 and 15.04 Å^2 for subunits I and II, respectively. The average B-value for the solvent was 34.16 Å^2. A Ramachandran plot of the nonglycinyl main-chain dihedral angles revealed Ala239 as the only significant outlier in each subunit. The strained ϕ and φ angles in this residue were previously attributed to the hydrogen bond formed between Ala239 and the nicotinamide ribose of the dinucleotide (*11*). The final R_{factor} for all measured X-ray data from 30 to 1.25-Å resolution was 19.5%. Relevant refinement statistics are given in Table 2. The subunits of the dimer superimpose, with a root-mean-square deviation of 0.80 Å for all main-chain backbone atoms, and the active sites are identical within experimental error.

Structural Determination of the E·NAD$^+$·L-3-phenyllactate Complex. Crystals of the E·NAD$^+$·L-3-phenyllactate complex were grown as described for the previous complex. The batch solution was prepared by mixing a 7.5 mg/mL solution of enzyme, buffered in 50 mM triethanolamine (pH 7.8)

Table 2: Least-Squares Refinement Statistics

	E•NADH•L-phenylalanine	E•NAD$^+$•L-3-phenyllactate
resolution limits (Å)	30−1.25	30−1.40
$R_{overall}$ (%)[a]/reflections/completeness (%)	19.5/215573/96	18.3/155817/97
$R_{working}$ (%)/reflections/completeness (%)	19.3/193973/86	18.0/140183/87
R_{free} (%)/reflections/completeness (%)	23.8/21600/10	22.9/15634/10
no. of protein atoms	5176	5157
no. of solvent atoms[b]	936	852
weighted root-mean-square deviations from ideality		
bond length (Å)	0.014	0.016
bond angle (deg)	2.53	2.40
planarity (trigonal) (Å)	0.007	0.009
planarity (other planes) (Å)	0.012	0.013
torsional angle (deg)[c]	14.7	15.0

[a] $R_{factors}$ are calculated as $\Sigma|F_o - F_c|/\Sigma|F_o|$, where F_o is the observed structure factor amplitude and F_c is the calculated structure factor amplitude. $R_{working}$ is the R_{factor} calculated for the reflections included in the least-squares refinement of the working model, R_{free} is for reflections that were randomly excluded from the least squares refinement procedure, and $R_{overall}$ is for all measured reflections. [b] These include 928 water molecules, 2 sodium ions, 4 potassium ions, 1 2-propanol, and 1 inorganic phosphate for the E·NADH·L-phenylalanine complex; and 844 water molecules, 1 sodium ion, 4 potassium ions, 3 2-propanols, and 1 inorganic phosphate for the E·NAD$^+$·L-3-phenyllactate complex. [c] Torsional angles were not restrained during refinement.

containing 100 mM NaCl and 10 mM NAD$^+$, with an equal volume of precipitant solution composed of 2.4 M Na$^+$/K$^+$ phosphate, 100 mM CHES (pH 8.7), 4% (v/v) 2-propanol, and 20 mM L-3-phenyllactate. These crystals also grew as rectangular, bladed tablets and belonged to the orthorhombic space group $P2_12_12_1$, with unit cell dimensions of $a = 64.6$ Å, $b = 110.4$ Å, and $c = 113.4$ Å and with a dimer in the asymmetric unit.

The crystals were prepared for data collection in a manner similar to that described for the previous complex. The synthetic mother liquor used to stabilize the crystals was composed of 1.5 M Na$^+$/K$^+$ phosphate, 50 mM CHES (pH 8.7), 2% (v/v) 2-propanol, 5 mM NAD$^+$, and 20 mM L-3-phenyllactate, and the crystals were transferred stepwise into 1.8 M Na$^+$/K$^+$ phosphate, 50 mM CHES (pH 8.7), 2% (v/v) 2-propanol, 5 mM NAD$^+$, 20 mM L-3-phenyllactate, and 10% (v/v) ethylene glycol. The crystals were cryocooled and were stored in liquid nitrogen until data collection.

X-ray data to 1.4-Å resolution were collected from a single crystal at the Structural Biology Center Beamline 19-ID. The data were collected as described for the previous complex, with the exception of an exposure rate of 4 s/frame. A total of 600 frames was collected, and the frames were processed by using DENZO and scaled by using SCALEPACK. From these frames, 735 380 reflections were integrated, which reduced to 156 183 unique reflections after scaling. Relevant X-ray data statistics are listed in Table 1.

The structure of the E·NAD$^+$·L-3-phenyllactate complex was solved by difference Fourier techniques. Alternate cycles of least-squares refinement and model building reduced the R_{factor} to 18.3% for all measured X-ray data from 30- to 1.4-Å resolution. Relevant refinement statistics for this complex are listed in Table 2. Residues Ser4, Asp55, and Met74 of subunit I were modeled in multiple conformations, as were residues Asp55, Met74, Ser192, Leu224, and Ile273 of subunit II. The average *B*-values for all main-chain backbone atoms were 18.41 and 15.12 Å^2 for subunits I and II, respectively. Alanines239 were again found to be the only significant outliers in the Ramachandran plot for the dimer. The main-chain backbone atoms of the two subunits superimpose, with a root-mean-square deviation of 0.78 Å. The electron density for the NAD$^+$ in subunit II was somewhat weak; the coordinates for this dinucleotide were included at 60% occupancy in the refinement. Otherwise, the active sites of the two subunits are identical.

Table 3: Kinetic Parameters of Alternate Nucleotide Substrates with *Rhodococcus* sp. M4 Phenylalanine Dehydrogenase

nucleotide	redox potential (mV)	K_m (mM)	V_{rel}	V/K_{rel}
NAD$^+$	−320	90 ± 20	100	100
NHD$^+$	−320	40 ± 30	70 ± 10	190 ± 140
NGD$^+$	−320	170 ± 40	90 ± 10	50 ± 10
thioNAD$^+$	−285	60 ± 10	100 ± 10	150 ± 30
3-pyridinealdehydeNAD$^+$	−263	50 ± 10	55 ± 5	100 ± 20
3-acetylpyridineNAD$^+$	−258	110 ± 10	350 ± 30	300 ± 40

RESULTS

Phenylalanine Dehydrogenase Purification. Approximately 25 mg of homogeneous *Rhodococcus* phenylalanine dehydrogenase can be purified 850-fold in a 44% overall yield from ca. 100 g of cells. Maintaining the ionic strength above $I = 0.05$ M throughout the purification was essential for enzyme stability. The subunit molecular mass was estimated by SDS−PAGE at 39 500 Da, and the apparent native molecular mass by gel filtration was approximately 150 000 Da by comparison to standards (Bio-Rad), suggesting a tetrameric quaternary structure. The isoelectric point was ca. 5.6, and the A_{280} for a 1.0 mg/mL solution was 0.56.

Equilibrium Constant. The apparent equilibrium constant, K_{eq}', for the phenylalanine dehydrogenase reaction was determined to be 3.98×10^{-6} M at pH 7.95 and 25 °C, using eq 1. The true equilibrium constant must take into account the proton released during the reaction (eq 12)

$$K_{eq} = K_{eq}'[H^+] = [NH_4^+][\phi\text{pyruvate}][NADH][H^+]/[NAD^+][\text{L-phenylalanine}] \quad (12)$$

This value was calculated to be 4.50×10^{-14} M^2, corresponding to a free energy change, $\Delta G°$, of 18.2 kcal/mol.

Alternate Nucleotide Substrates. Table 3 lists the kinetic parameters, *V* and *V*/*K*, of the alternate nucleotide substrates tested in the forward reaction relative to NAD$^+$. 2′-phos-

Table 4: Steady-State Inhibition by Product Inhibitors

variable substrate	product inhibitor	K_{is} (μM)	K_{ii} (μM)	fixed substrate	inhibn pattern[a]
NAD^+	NADH	7.9 ± 1.4		L-phenylalanine	c
L-phenylalanine	NADH	0.09 ± 0.02	0.05 ± 0.01	NAD^+	nc
NAD^+	ϕpyruvate	1.1 ± 0.4	2.6 ± 0.3	L-phenylalanine	nc
L-phenylalanine	ϕpyruvate	0.4 ± 0.1	0.9 ± 0.1	NAD^+	nc
NAD^+	NH_4^+	1200 ± 800	5200 ± 4200	L-phenylalanine	nc
L-phenylalanine	NH_4^+			NAD^+	n/d

[a] c, competitive inhibition; nc, noncompetitive inhibition; and n/d, not determined.

Table 5: Steady-State Inhibition by Dead-End Inhibitors

variable substrate	dead-end inhibitor	K_{is} (mM)	K_{ii} (mM)	fixed substrate(s)	inhibition[a]
L-phenylalanine	D-phenylalanine	0.4 ± 0.1	0.17 ± 0.02	NAD^+	nc
NAD^+	D-phenylalanine	0.7 ± 0.3	0.7 ± 0.1	L-phenylalanine	nc
L-phenylalanine	L-phenyllactate	7.5 ± 0.3		NAD^+	c
L-phenylalanine	phenylethylamine	7.4 ± 1.0		NAD^+	c
L-phenylalanine	phenylpropionate	0.71 ± 0.03		NAD^+	c
L-phenylalanine	*trans*-cinnamate	1.6 ± 0.1		NAD^+	c
phenylpyruvate	D-phenylalanine	0.037 ± 0.002		NADH, NH_4^+	c
NH_4^+	D-phenylalanine	0.5 ± 0.1	2 ± 5	NADH, phenylpyruvate	nc
phenylpyruvate	L-phenyllactate	13 ± 1		NADH, NH_4^+	c
NH_4^+	L-phenyllactate	90 ± 10	70 ± 10	NADH, phenylpyruvate	nc
NADH	L-phenyllactate		42 ± 4	phenylpyruvate, NH_4^+	uc
phenylpyruvate	phenylethylamine	15 ± 2		NADH, NH_4^+	c
phenylpyruvate	phenylpropionate	3.2 ± 0.5		NADH, NH_4^+	c
phenylpyruvate	*trans*-cinnamate	4 ± 1		NADH, NH_4^+	c

[a] c, competitive inhibition; nc, noncompetitive inhibition; and uc, uncompetitive inhibition.

phorylated nucleotides, for example, $NADP^+$, were not substrates for the enzyme.

Initial Velocity, Product, and Dead-End Inhibition Studies. In the forward direction, the initial velocity studies obtained by varying the concentration of L-phenylalanine at several fixed levels of NAD^+ exhibited an intersecting pattern on a double-reciprocal plot (data not shown). The K_m value of NAD^+ was determined to be 1.4 mM, and the K_m value for L-phenylalanine was determined to be 5.5 mM. Initial velocity studies were performed in the reverse direction for all combinations of two varied substrates, at saturating levels of the third. When the variable substrates were either NADH and phenylpyruvate or NH_4^+ and phenylpyruvate, the patterns were intersecting, indicating a sequential addition of these substrates. The initial-velocity pattern obtained with variable concentrations of NADH and NH_4^+ exhibited parallel lines at a saturating concentration of phenylpyruvate. The K_m values determined for these substrates were 0.03 mM for NADH, 0.12 mM for phenylpyruvate, and approximately 47 mM for NH_4^+. Table 4 summarizes the K_i values and types of inhibition displayed by a series of product inhibitors.

Table 5 summarizes the types of inhibition displayed by a variety of dead-end inhibitors (shown in Figure 1). The best competitive inhibitor in the forward reaction was 3-phenylpropionate, with a K_i of 0.7 mM. In the reverse direction, D-phenylalanine was the best competitive inhibitor with a K_i of 0.04 mM. Most compounds tested were linear, competitive inhibitors against both L-phenylalanine and phenylpyruvate, with two exceptions. Phenylglycine is a poor inhibitor versus L-phenylalanine, and D-phenylalanine displayed unexpected noncompetitive inhibition versus L-phenylalanine.

Stereochemistry of Hydride Transfer. The mass spectrum of authentic L-phenylalanine or L-phenylalanine synthesized enzymatically from phenylpyruvate, NH_4^+, and NADH gave a molecular ion at $m/z = 165.9$ (data not shown). The mass spectrum of L-phenylalanine synthesized enzymatically from phenylpyruvate, NH_4^+, and [4*S*-^{2}H]-NADH showed a molecular ion at $m/z = 166.9$, corresponding to [2-^{2}H]-phenylalanine (data not shown).

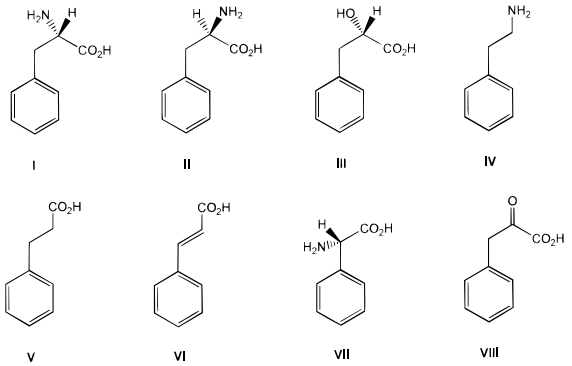

FIGURE 1: Chemical structure of L-phenylalanine and L-phenylalanine substrate analogues used in this study. I = L-phenylalanine, II = D-phenylalanine, III = L-3-phenyllactate, IV = 2-phenylethylamine, V = 3-phenylpropionate, VI = *trans*-cinnamate, VII = phenylglycine, and VIII = phenylpyruvate.

pH Dependence of the Kinetic Constants. Table 6 lists all of the p*K* values obtained from fits of the various pH profiles in the forward and reverse directions. Figure 2A illustrates the pH dependence of *V* in the forward direction, and the best fit of the data was obtained when eq 3 was used, suggesting the presence of two ionizable groups which must be deprotonated for catalysis in the forward direction. These two enzyme groups exhibited p*K* values (7.2 ± 0.1) too close to resolve. Figure 2B illustrates the pH dependence of log V/K_{L-Phe}. Two groups, exhibiting p*K* values of 7.0 ± 0.5 and 8.7 ± 0.4, must be unprotonated, while a third group,

Table 6: pH Dependence of the Kinetic Parameters of Phenylalanine Dehydrogenase

parameter	eq fitted	$pK_0 - pK_1$	pK_1	pK_2
log V/K_{NAD}	2		9.1 ± 0.2	11.0 ± 0.3
log $V/K_{L-phenylalanine}$	5	7.0 ± 0.5	8.7 ± 0.3	10.4 ± 0.3
log $V_{forward}$	3		7.2 ± 0.2	7.2 ± 0.2
log V/K_{NADH}	2		7.3 ± 0.2	9.9 ± 0.2
log $V/K_{phenylpyruvate}$	2		7.6 ± 0.2	9.3 ± 0.2
log $V/K_{ammonia}$	2		9.4 ± 0.2	10.0 ± 0.2
log $V_{reverse}$	2		8.1 ± 0.3	9.4 ± 0.2
pK_d(phenylpyruvate)	4		7.6 ± 0.3	
pK_i(phenylpropionate)	4		9.9 ± 0.2	

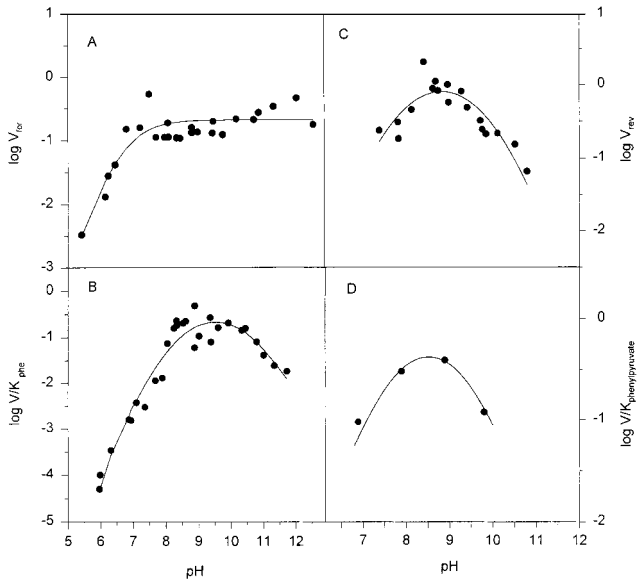

FIGURE 2: pH profiles. (a) pH dependence of log $V_{forward}$ in the direction of phenylalanine oxidation. Experimental points are shown, and the smooth curve is a fit of the data to eq 3. (b) pH dependence of V/K_{L-Phe}. Experimental points are shown, and the smooth curve is a fit of the data to eq 5. (c) pH dependence of log $V_{reverse}$ in the direction of phenylpyruvate reductive amination. Experimental points are shown and the smooth curve is a fit of the data to eq 2. (d) pH dependence of $V/K_{phenylpyruvate}$. Experimental points are shown, and the smooth curve is a fit of the data to eq 2.

exhibiting a pK value of 10.4 ± 0.3, must be protonated for optimal binding.

Figure 2C shows the pH dependence of the maximum velocity in the reverse direction. Fits of log V versus pH yielded pK values of 8.1 ± 0.3 and 9.4 ± 0.3 for groups which must be deprotonated and protonated, respectively, for optimal activity in this direction. The pH dependence of log V/K_{NH3} was also bell-shaped, and fits of the data-yielded pK values of 9.4 ± 0.1 and 10.0 ± 0.2 for groups which must be deprotonated and protonated, respectively, for optimal binding and reaction in this direction (data not shown).

The log $V/K_{phenylpyruvate}$ pH profile is bell-shaped and depends on the ionization of two groups, one exhibiting a pK value of 7.5 ± 0.2 that must be deprotonated and the other, a group at 9.3 ± 0.3 that must be protonated, for optimal binding (Figure 2D). 3-Phenylpropionate was chosen as the competitive inhibitor versus phenylpyruvate, whose pH dependence would be evaluated because of its relatively low K_i. When the pK_i value of phenylpropionate was determined as a function of pH, the protonation of a single

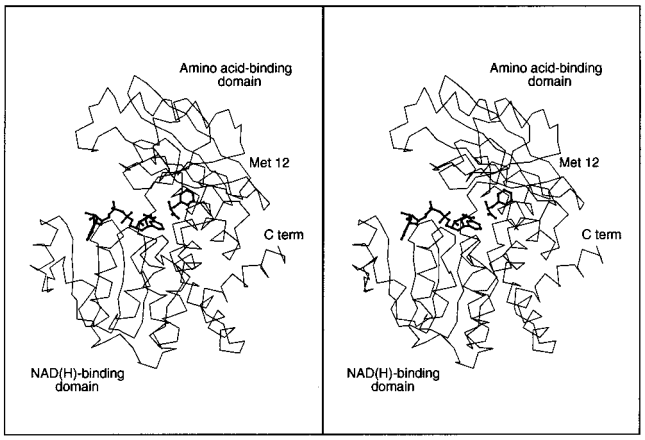

FIGURE 3: α-Carbon trace of one subunit of L-phenylalanine dehydrogenase. NADH and L-phenylalanine are shown as ball-and-stick representations. This figure, Figure 5, and Figure 6 were produced using the program MOLSCRIPT (*37*).

residue exhibiting a pK value of 9.9 ± 0.2 was observed to decrease the K_i value (data not shown).

*Molecular Structure of the E·NADH·*L*-phenylalanine and E·NAD$^+$·*L*-3-phenyllactate Complexes*. The overall molecular structure of the E·NADH·L-phenylalanine and E·NAD$^+$·L-3-phenyllactate complexes is like that of the two previously reported ternary complexes of phenylalanine dehydrogenase (*11*), such that the superposition of the polypeptide backbone atoms on those of the E·NAD$^+$·phenylpyruvate structure yields root-mean-square deviations of 0.292 and 0.196 Å^2 for the E·NADH·L-phenylalanine and E·NAD$^+$·L-3-phenyllactate models, respectively. An α-carbon trace of subunit I of the E·NADH·L-phenylalanine complex is shown in Figure 3. In the orientation shown, the dinucleotide is observed along the bottom surface of the active site cleft, and the amino acid substrate is seen at the cleft's base. As indicated earlier, the active sites within the dimer are virtually identical in both of the complexes reported here. For the sake of simplicity, our discussion will refer to subunit I of each complex.

The electron density corresponding to the dinucleotide and the ligand in the two complexes is displayed in Figure 4, and for both complexes, the fit into the density is unambiguous. Both nicotinamide rings adopt the *syn*-conformation about the glycosidic bond, as was observed previously in the complex of the enzyme with NAD$^+$ and 3-phenylpropionate. This conformation is generally observed for "*B*" side-specific enzymes, which transfer the 4*S* hydrogen of NADH.[2]

The interactions that bind the dinucleotides are practically identical for the E·NADH·L-phenylalanine and the E·NAD$^+$·L-3-phenyllactate complexes. The binding interactions of the two ligands, however, are dramatically different, as illustrated in the active-site representations of Figure 5. In the E·NADH·L-phenylalanine complex (Figure 5a), the orientation of

[2] In the previously determined structure of the E·NAD$^+$·phenylpyruvate complex, the nicotinamide ring is rotated approximately 180° about the glycosidic bond and is, thus, in the *anti*-conformation. This conformation does not allow direct hydride transfer to and from the *B* side of the dinucleotide (*11*). The large active site appears to easily accommodate flipping of the nicotinamide ring between the *syn*- and *anti*-conformers; however, the significance of this conformational flipping, if any, is currently unknown.

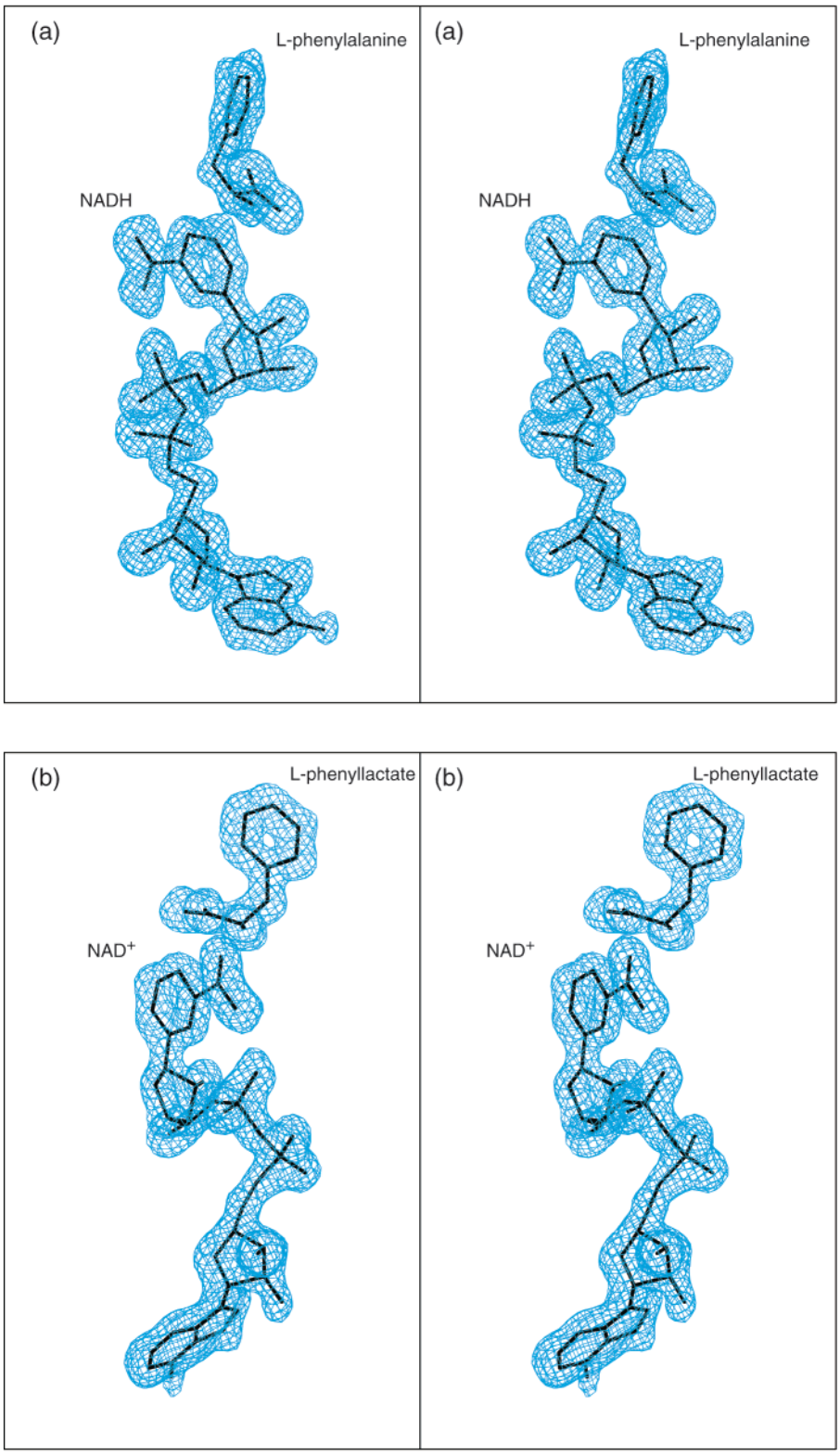

FIGURE 4: Representative electron density for the nucleotides and the ligands. The maps shown were calculated with coefficients of the form ($F_o - F_c$), where F_o was the native structure factor amplitude, and F_c was the calculated structure factor amplitude from the models lacking the coordinates for the dinucleotides and the ligands. (a) Electron density corresponding to NADH and L-phenylalanine. The map was calculated using X-ray data from 30- to 1.25-Å resolution and contoured at 3σ. In the orientation shown, the *B* side of the nicotinamide ring is toward the viewer. (b) Electron density corresponding to NAD^+ and L-3-phenyllactate. The map was calculated using X-ray data from 30- to 1.4-Å resolution and contoured at 3σ. To provide a clearer view, the electron density in this panel is rotated relative to that in the above panel by approximately 80° in a counterclockwise direction about the long axis of the drawing. In this orientation, the *B* side of the nicotinamide ring is away from the viewer. This figure was produced with the program FROST (G. Wesenberg, University of Wisconsin).

L-phenylalanine is nearly perfect for hydride transfer to the dinucleotide, with a distance of 3.54 Å separating the Cα of L-phenylalanine and the C4 of the nicotinamide ring. The α-amino group of this ligand is within hydrogen-bonding

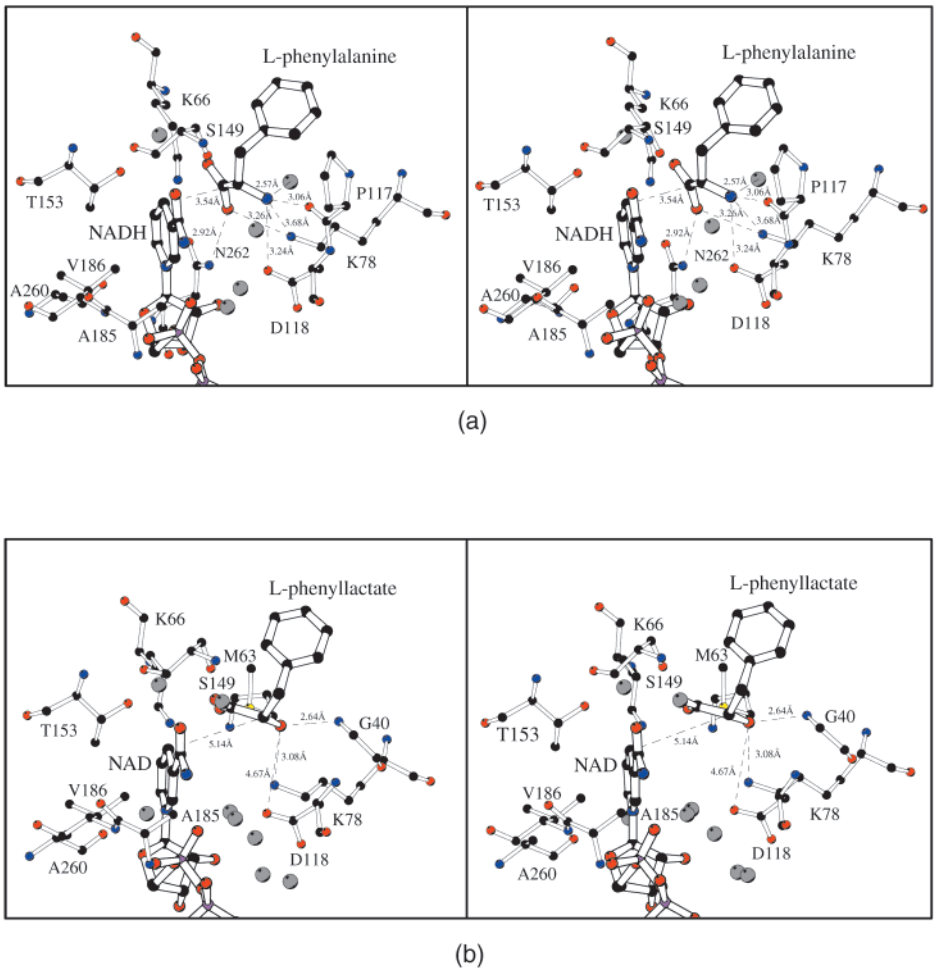

FIGURE 5: Closeup views of the L-phenylalanine dehydrogenase active site when complexed with NADH and L-phenylalanine (a) and NAD^+ and L-3-phenyllactate (b). In each panel, those amino acid residues located within approximately 3.3 Å of the dinucleotide and the ligand are displayed. Selected atomic distances are indicated by dashed lines.

distance of the carboxyl group of Asp118, the carbonyl oxygen of Pro117, and an active-site water molecule. The α-hydroxyl group of L-3-phenyllactate does not form these same hydrogen bonds, but instead interacts with the ϵ-amino group of Lys78 and the main-chain nitrogen of Gly40 (Figure 5b). Relative to that of L-phenylalanine, the Cα of L-3-phenyllactate is positioned deeper inside the active-site cleft. The distance of this carbon to the C4 of the nicotinamide is 5.14 Å, and its orientation is such that direct transfer of its hydrogen to the nicotinamide is not possible. The binding interactions of the α-carboxylate group of the ligands also differs between the two complexes. In the E•NADH•L-phenylalanine complex, the α-carboxylate interacts with the ϵ-amino groups of Lys66 and Lys78 and the carboxamide of Asn262. In the L-3-phenyllactate-containing complex, the α-carboxylate is rotated such that only the interaction with Lys66 is maintained.

DISCUSSION

The cleavage of the Cα−N bond of L-amino acids is accomplished by a variety of enzymes. These include the pyridoxal phosphate-dependent transaminases, of which many have been described using various combinations of amino acid and keto acid substrates (*23*). Deaminations of L-amino acids by elimination of ammonia to generate the unsaturated acid are typified by the reactions catalyzed by phenylalanine ammonia-lyase (*24*) and aspartase (*25*). A third, and common, catalytic strategy is exemplified by the amino acid dehydrogenases, which generate ammonia and reduced pyridine dinucleotide from the oxidative deamination of the amino acid (*26*). The latter have been of mechanistic interest for over three decades, but only recently have the three-dimensional structures of any amino acid dehydrogenase been determined. At present, the structures of L-glutamate dehydrogenase (*13*), L-leucine dehydrogenase (*14*), L-alanine dehydrogenase (*27*), L-phenylalanine dehydrogenase (*11*), and *meso*-diaminopimelate dehydrogenase (*15*) have been reported. *meso*-Diaminopimelate dehydrogenase is unique among this group, because it catalyzes the oxidative deamination of a D-amino acid.

The rapid purification to homogeneity of phenylalanine dehydrogenase could be accomplished from cultures of *Rhodococcus* sp. M4 grown in the presence of L-phenylalanine as the sole nitrogen source. The purification protocol that was developed takes advantage of the highly selective binding of phenylalanine dehydrogenase to the Red A dye matrix, which has been used previously to purify other NAD^+-dependent phenylalanine dehydrogenases (*4*, *28*). The specific activity of 935 U/mg for the *Rhodococcus* sp. M4 phenylalanine dehydrogenase compares favorably to the

values reported for phenylalanine dehydrogenase from *Bacillus badius* (68 U/mg, *29*) and *Rhodococcus maris* (162 U/mg, *28*). The homogeneous *Rhodococcus* sp. M4 enzyme can be stored in 50% glycerol without loss of activity for more than 6 months, in contrast to other phenylalanine dehydrogenases which have been reported to lose activity rapidly (*3, 28*).

Phenylalanine dehydrogenases exhibit a narrow range of subunit molecular masses between 36 and 42 kDa, and the 39.5 kDa *Rhodococcus* sp. M4 enzyme falls into the middle of this range. There is considerable variation in the quaternary structures of these enzymes. The enzymes from *B. badius*, *Bacillus sphaericus*, and *Sporosarcina ureae* have been reported to be octomers (*2, 29*), the *Thermoactinomyces intermedius* enzyme has been reported to be a hexamer (*4*), the *R. maris* K-18 enzyme has been reported to be a dimer (*28*), and the *Nocardia* sp. 239 enzyme has been reported to be a monomer (*3*). The quaternary structure of the *Rhodococcus* sp. M4 phenylalanine dehydrogenase appears to be dependent on ionic strength and/or the conformational state of the enzyme. When the apo-enzyme is subjected to size-exclusion chromatography under low-salt conditions (50 mM NaCl), it behaves as a tetramer. However, when crystallized as a ternary dead-end complex under conditions of high salt (1.2 M Na^+/K^+ phosphate), the enzyme clearly packs in the crystalline lattice as a dimer, with the monomeric subunits related by a noncrystallographic 2-fold axis. The generation of a tetrameric species within the lattice by crystallographic symmetry operations is not possible, because each of the 2-fold rotational axes of the $P2_12_12_1$ lattice also contains a translational element. Amino acid dehydrogenases are known to undergo a conformational transition from an "open" form to a "closed" form upon the binding of substrates or inhibitors in the amino acid binding site (*13, 15*). Superposition of the open and closed forms of *meso*-diaminopimelate dehydrogenase on the structures we have determined demonstrates that the ternary complexes of phenylalanine dehydrogenase represent the closed conformation (data not shown). At the ionic strength used for the size-exclusion experiment, the enzyme is presumably in its open conformation. At present, no structures have been obtained for either the apo-enzyme or the binary complex with dinucleotide, but preliminary analysis of two different crystal forms grown from poly(ethylene glycol) in the presence of NAD^+ suggests that both crystals contain a tetramer in the asymmetric unit (unpublished data). The amino acid binding site is expected to be unoccupied in these crystals, and the enzyme should, therefore, assume the open conformation.

The equilibrium constant of 4.50×10^{-14} M^2, determined for the phenylalanine dehydrogenase reaction, is typical of other amino acid dehydrogenases (*26*). Although amino acid synthesis is favored thermodynamically, the physiological role of the enzyme in this soil bacterium is likely to be the degradation of L-phenylalanine for use as a carbon and nitrogen source. This reasoning is supported by the observation that enzyme levels are substantially increased in the presence of L-phenylalanine in the media (*5*) and that *Rhodoccocus* sp. M4 can grow on media with 1% L-phenylalanine as the sole carbon and nitrogen source.

The specificity for alternate amino acid and keto acid substrates has been determined for *Rhodococcus* phenylalanine dehydrogenase (*30*); however, the ability of alternate dinucleotide substrates to support phenylalanine oxidation has not been reported. The enzyme exhibits a strict specificity against 2′-phosphorylated dinucleotides but broad specificity for nonphosphorylated dinucleotides (Table 3). The 2′- and 3′-hydroxyl groups of the adenosyl ribose form strong hydrogen bonds with the carboxylate of Asp205 in the crystal structures (distances of 2.81 and 2.69 Å, respectively), and these hydrogen bonds would be disrupted by the presence of a 2′-phosphate. The *V*/*K* values for NHD^+, thioNAD^+, and 3-acetylpyridineNAD^+ are all greater than for NAD^+. There is no correlation between the maximum velocities exhibited by various NAD^+ analogues and their redox potentials, which suggests that chemistry is unlikely to be rate-limiting in the direction of phenylalanine oxidation.

Rhodococcus sp. M4 phenylalanine dehydrogenase catalyzes the direct hydride transfer of the 4*S* hydrogen of NADH to the *re* face of the imine of phenylpyruvate to form L-phenylalanine. The stereospecificity of hydride transfer is a conserved characteristic of amino acid dehydrogenases, with most enzymes catalyzing the transfer of the 4*S* hydrogen to the imine of the keto acid. The exceptions to this rule include L-alanine dehydrogenase (*31, 32*), L-lysine ϵ-dehydrogenase (*33*), and *meso*-diaminopimelate dehydrogenase (*15*). The stereospecificity of the *Rhodococcus* enzyme is concordant with the position of NADH and L-phenylalanine in the three-dimensional structure reported here and confirms that this dead-end complex represents a stereochemically relevant complex.

The importance of each of the groups on the substrate to binding was examined using structurally similar dead-end inhibitors. 3-Phenylpropionic acid (hydrocinnamic acid) is a competitive inhibitor versus either L-phenylalanine or phenylpyruvate and exhibits a K_i value versus L-phenylalanine that is lower than the K_m for L-phenylalanine. The tight binding of 3-phenylpropionate suggests that the interactions observed in the crystal structure between the amino group of L-phenylalanine and the enzyme are unnecessary for correct binding. This interpretation of the kinetic data is substantiated by the superposition of the three-dimensional structures of the E·NADH·L-phenylalanine and E·NADH·3-phenylpropionate complexes (Figure 6), which shows that the position of 3-phenylpropionate in the active site is nearly identical to that of L-phenylalanine. The *trans*-isomer of cinnamic acid (*trans*-3-phenyl-2-propenoic acid) is less effective than 3-phenylpropionate as an inhibitor, suggesting that this rigid inhibitor is poorly accommodated in the active site compared to phenylpropionate, which binds to the enzyme in a *cis*-oid conformation (*11*, and Figure 6). 2-Phenylethylamine is a poor inhibitor, with an inhibition constant an order of magnitude higher than that for 3-phenylpropionate. This observation signifies the importance of the α-carboxylate group of the substrate for binding. D-Phenylalanine exhibits unusual behavior, binding tightly as a competitive inhibitor versus phenylpyruvate ($K_i = 37$ μM) but an order of magnitude less tightly as a noncompetitive inhibitor versus L-phenylalanine ($K_{is} = 370$ μM). There are at least two possible explanations that may account for this behavior: D-phenylalanine may bind more tightly to the E·NADH complex than to the E·NAD^+ complex, and it may bind as a mimic of the intermediate carbinolamine.

The kinetic mechanism of *Rhodococcus* sp. M4 phenylalanine dehydrogenase is ordered bi-ter with NAD^+ and L-phenylalanine binding in that order to form a ternary

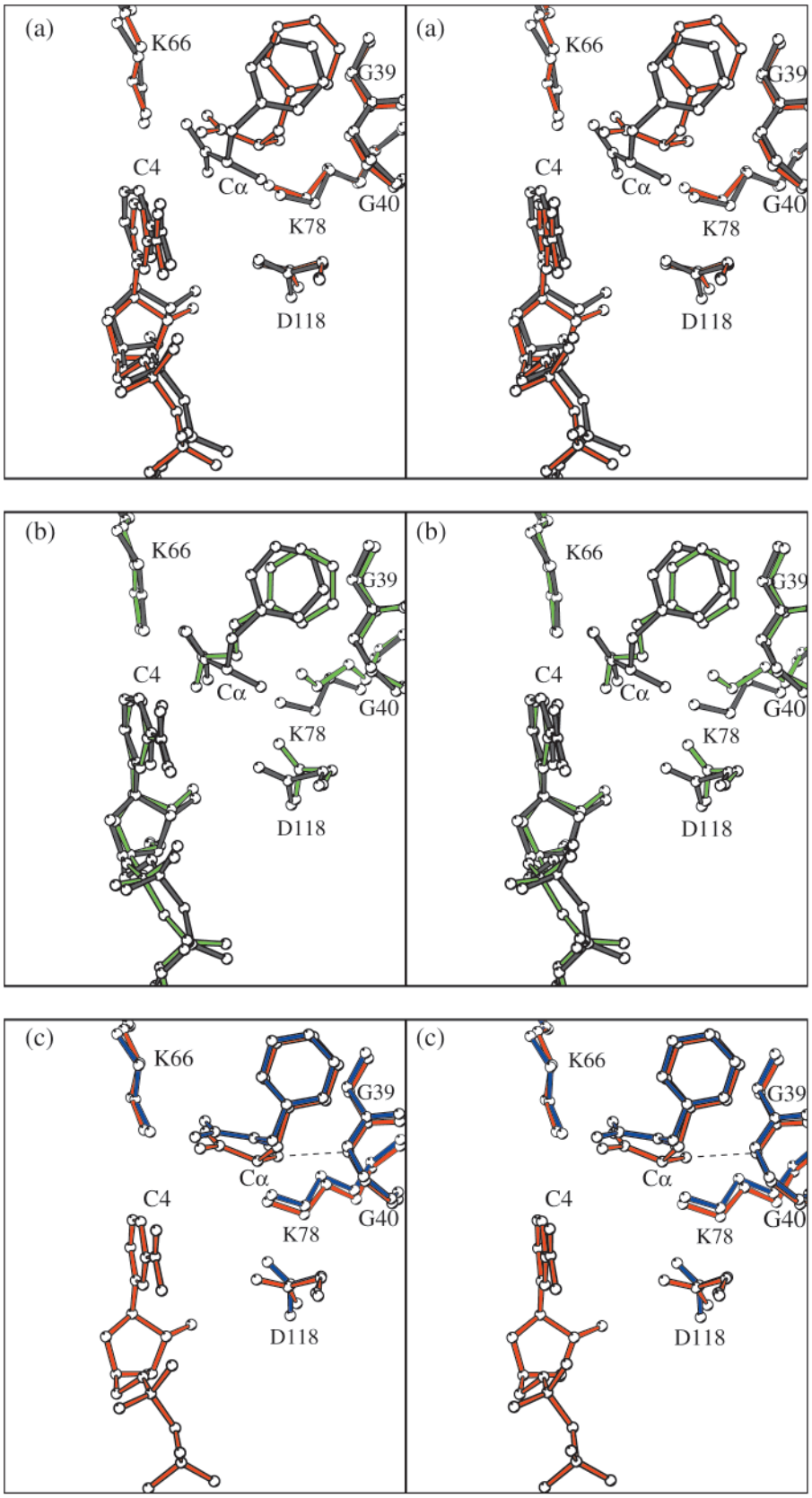

FIGURE 6: Closeup views of the ligand orientations in the four inhibitory ternary complexes of L-phenylalanine dehydrogenase. The coordinates of the three ternary complexes containing NAD^+ were superimposed on those of the NADH-containing complex to create the overlays displayed. (a) Overlay of the E·NADH·L-phenylalanine and E·NAD^+·L-3-phenyllactate complexes. Residues and ligands corresponding to the E·NADH·L-phenylalanine complex are in gray, and those corresponding to the E·NAD^+·L-3-phenyllactate complex are in red. (b) Overlay of the E·NADH·L-phenylalanine (gray) and the E·NAD^+·3-phenylpropionate (green) complexes. (c) Overlay of the E·NAD^+·L-3-phenyllactate (red) and E·NAD^+·phenylpyruvate (blue) complexes. The NAD^+ in the latter complex binds in a nonproductive fashion and has been omitted for clarity. The dashed line indicates the hydrogen bond of length 2.64 Å between the main-chain nitrogen of Gly40 and the α-hydroxyl moiety of L-3-phenyllactate. The hydrogen bond of length 2.96 Å between the keto oxygen of phenylpyruvate and N of Gly40 is obscured in the drawing.

complex, followed by the ordered released of NH_4^+, phenylpyruvate, and NADH:

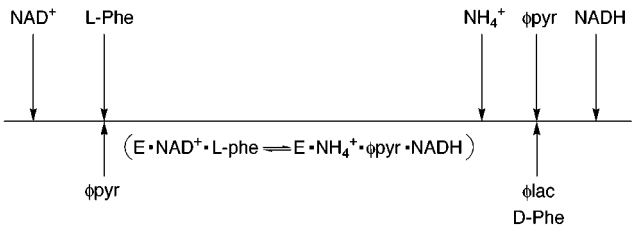

This ordered-binding sequence has been reported for other amino acid dehydrogenases (*26*), including the *R. maris* phenylalanine dehydrogenase (*28*). Ohshima et al. (*4*) reported that the *T.intermedius* phenylalanine dehydrogenase releases products in the order of phenylpyruvate, ammonia, and NADH. The ordered release of NH_4^+, phenylpyruvate, and NADH for the *Rhodococcus* dehydrogenase is supported by the parallel initial velocity pattern obtained by varying NH_4^+ and NADH at a fixed, saturating level of phenylpyruvate. These initial velocity studies were confirmed through the analysis of the inhibition patterns exhibited by the dead-end inhibitors D-phenylalanine and L-3-phenyllactate (Table 5). Both of these inhibitors are competitive versus phenylpyruvate, and both exhibit uncompetitive inhibition versus NADH and noncompetitive inhibition versus NH_4^+, the three patterns expected for the ter-reactant portion of the kinetic mechanism shown in the above scheme. The unexpected noncompetitive inhibition displayed by phenylpyruvate versus the varied substrate L-phenylalanine (Table 4) suggests that an abortive E·NAD^+·phenylpyruvate complex can form. This suggestion has been experimentally borne out, because this complex has been prepared, crystallized, and structurally characterized (*11*).

The pH dependence of the kinetic parameters V_{max}, V_{max}/K_m, and K_i describes the ionization behavior of residues in the active site that are required for optimal activity and substrate or inhibitor binding, as well as the preferred protonation state of substrate molecules (*34*). The p*K* value of 9.9 accurately represents the p*K* for the enzymic group that must be protonated for 3-phenylpropionate binding, because the pH dependence of the K_i of a competitive inhibitor is free of any kinetic effects which may perturb the intrinsic p*K* value exhibited by the group (*34*). The three-dimensional structure of the E·NAD^+·3-phenylpropionate complex allows us to unambiguously identify this group as Lys66, which interacts electrostatically with the carboxyl group of the inhibitor. This residue is completely conserved in all phenylalanine, leucine, and glutamate dehydrogenase sequences, and the corresponding residue in the *Clostridium symbiosum* glutamate dehydrogenase-L-glutamate complex (K113) makes a similar interaction with the α-carboxylate of bound glutamate (*13*).

The pH dependence of V/K_{L-Phe} is dependent on the ionization state of three groups. The group exhibiting the highest p*K* value, 10.4, must be protonated, and is likely to be the side chain of Lys66, which binds the α-carboxyl group of 3-phenylpropionate and L-phenylalanine. The second group observed in the V/K_{L-Phe} pH profile must be unprotonated and exhibits a p*K* of 8.7. This p*K* may represent the ionization of the α-amino group of L-phenylalanine (p*K* = 9.3); however, the weak binding of 2-phenylethylamine compared to 3-phenylpropionate argues that the amino group contributes little to binding. An alternative assignment that we favor for the group demonstrating this ionization behavior is Lys78, which is completely conserved in all L-amino acid dehydrogenases and is observed to interact with the α-carboxylate of L-phenylalanine and an active-site water molecule. The third group in the pH profile displays a p*K* value of 7.0 and must be unprotonated. We believe this p*K* value is attributable to Asp118, a highly conserved residue observed in the active sites of both phenylalanine and glutamate dehydrogenase. The assignment of these protonation states to Lys78 and Asp118 is supported by the pH dependence of *V* in the direction of phenylalanine oxidation. This profile indicates the presence of two enzymic groups, each with a p*K* of 7.2, that must be deprotonated for optimal catalytic activity.

The pH dependence of *V* in the direction of phenylalanine synthesis requires that one enzymic group with a p*K* of 9.4 must be protonated, while another enzymic group exhibiting a p*K* value of 8.1 must be unprotonated. We assign the higher p*K* value and a positive charge to Lys78, the residue we observed previously to form a strong hydrogen bond (distance of 3.1 Å) with the carbonyl oxygen of phenylpyruvate (*11*). We believe the lower p*K* of 8.1 is attributable to the side chain of Asp118 and, thus, assign a negative charge to the carboxyl group of this residue. In the reaction catalyzed by glutamate dehydrogenase, the homologous aspartate residue (D165 in the *C. symbiosum* enzyme) has been assigned a neutral charge in the E·NADH·α-ketoglutarate complex (*13*), primarily on the basis of the pH dependence of the K_i value for α-ketoglutarate and the dead-end inhibitor, oxalylglycine (*35*). However, the pH dependence of the K_i value for phenylpyruvate reveals that either the deprotonation of Lys78 or the protonation of Asp118 increases the K_i value of phenylpyruvate (Figure 2D). This difference in charge represents an important distinction between the mechanisms of these two amino acid dehydrogenases and necessitates the modification of the mechanism we presented earlier for phenylalanine dehydrogenase (*11*) in which Asp118 was shown to be protonated and interacting with the carbonyl oxygen of bound phenylpyruvate.

The observation of the catalytic water molecule in the E·NADH·L-phenylalanine complex supports its presence at the start of the oxidative reaction, as proposed in our previous mechanism. This water molecule has well-defined electron density (*B*-value = 23.96 $Å^2$), and it forms strong hydrogen bonds with the α-amino group of the amino acid substrate and the ϵ-amino group of Lys78, the distances of which are 2.57 and 2.62 Å, respectively. The angle between these interactions is 90.6°, yielding a distance of 3.68 Å between the amino groups of the substrate and the catalytic lysine. We previously proposed that the deprotonation of L-phenylalanine prior to its oxidation occurs through direct proton transfer to this lysine. The arrangement of hydrogen bonds observed in the E·NADH·L-phenylalanine complex seems to indicate, however, that proton transfer between the substrate and the lysine is not direct but instead is mediated through the catalytic water molecule. In their mechanism for glutamate dehydrogenase, Stillman et al. proposed that L-glutamate is deprotonated by the catalytic aspartate (*13*). The position of the carboxylate of Asp118 in the E·NADH·L-phenylalanine complex suggests that it functions to stabilize

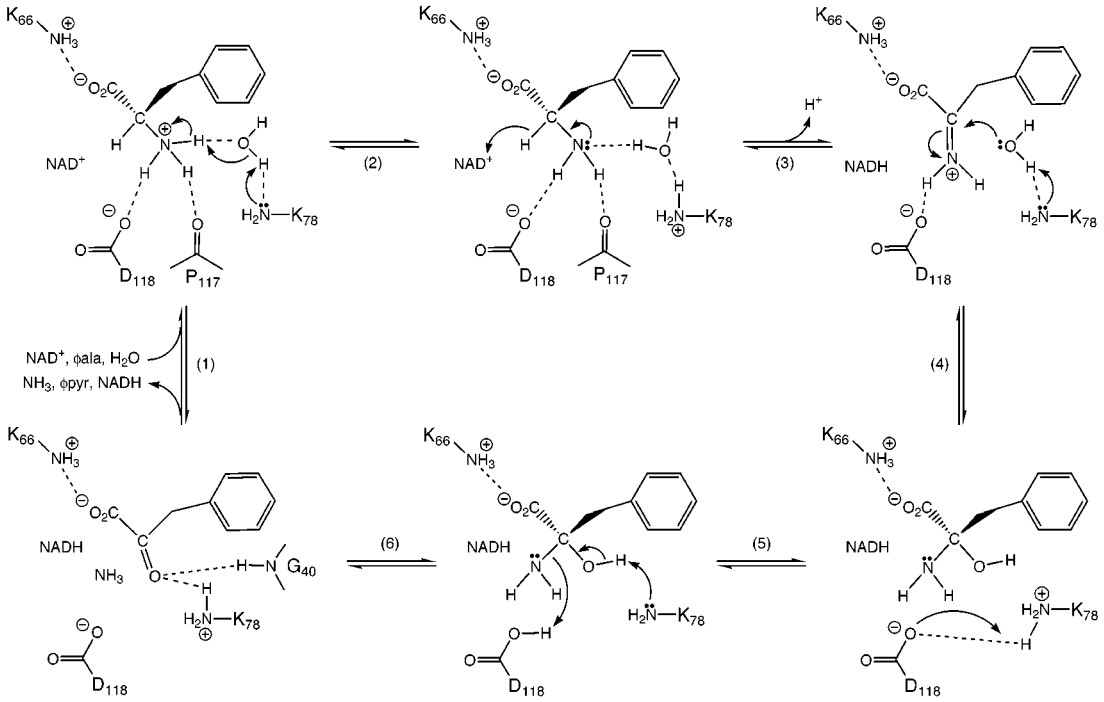

FIGURE 7: Chemical mechanism for L-phenylalanine dehydrogenase derived from kinetic and structural analyses. The oxidative deamination of L-phenylalanine to phenylpyruvate is shown as the forward reaction.

the positively charged imino intermediate that is formed upon the oxidation of the amino acid. As a higher degree of stabilization is afforded by an electrostatic interaction between the imine and a negatively charged carboxyl group, we favor the water-mediated proton transfer to Lys78 over deprotonation by Asp118 as the mechanism for deprotonation of the amino acid substrate.

We have combined our kinetic and structural findings to reformulate our chemical mechanism for the reversible, NAD^+-dependent, oxidative deamination reaction catalyzed by L-phenylalanine dehydrogenase. As illustrated in Figure 7, the first step of this mechanism entails the binding of NAD^+, L-phenylalanine, and the catalytic water molecule to the active site. The amino acid binds in this initial complex as the protonated amine, and Lys78 and Asp118 are unprotonated. The α-amino group of the substrate forms hydrogen bonds with Asp118, Pro117, and the water molecule. The α-carboxylate of the substrate interacts electrostatically with Lys66 and forms hydrogen bonds with Asn262 and Lys78. In step 2, L-phenylalanine is deprotonated via a water-mediated proton shuttle to Lys78. Hydride transfer from the deprotonated amino acid to NAD^+ occurs subsequently in step 3. As depicted in the figure, this hydride transfer is accompanied by proton loss from Lys78. The loss of a proton during the oxidation of L-phenylalanine is mandated by the requirement of a negative charge on the carboxyl group of Asp118 in the E·NH_4^+·phenylpyruvate·NADH product complex. As indicated earlier, kinetic evidence suggests that the catalytic aspartic acid of glutamate dehydrogenase is uncharged in the analogous E·NH_4^+·α-ketoglutarate·NADH product complex, and as such, proton loss to preserve the negative charge on this residue is not a requirement of the mechanism of glutamate dehydrogenase. Loss of a proton from the catalytic lysine of glutamate dehydrogenase to the solvent has, however, been demonstrated to be a prerequisite for binding the catalytic water molecule. The transient-state kinetic studies of Fisher and co-workers indicate that this proton is released after the hydride-transfer step in the reaction catalyzed by the *C. symbiosum* enzyme but before the hydride-transfer step in the reaction catalyzed by the beef liver enzyme (*36*). We expect transient-state kinetic studies of the phenylalanine dehydrogenase reaction will aid in the clarification of the mechanism of the proton loss we show in step 3 of our proposed reaction scheme, because presently the fate of this proton and the time of its release relative to hydride transfer cannot be established from our available data.

Iminophenylpyruvate, in protonated form, is the first intermediate generated upon the oxidation of L-phenylalanine. The substituents are oriented about the Cα in trigonal fashion; thus the imine nitrogen of the intermediate lies at a position between that occupied by the α-amino group and that occupied by the Hα of L-phenylalanine. Barring a substantial change in the polypeptide backbone, the distance between the imine nitrogen and the carbonyl oxygen of Pro117 is too far for any significant interaction, and as such, the intermediate is stabilized solely by an electrostatic interaction with the ionized carboxyl of Asp118. This interaction also positions the intermediate for addition of the catalytic water, which follows in step 4 and is assisted by Lys78. The reaction yields a tetrahedral carbinolamine, the second intermediate along the oxidative pathway. Proton transfer from Lys78 to Asp118 (step 5) allows both of these residues to facilitate the elimination of ammonia from the intermediate (step 6) to form the product α-keto acid, phenylpyruvate, and complete the catalytic cycle.

The difference in the orientation and binding interactions of L-phenylalanine and phenylpyruvate in the active site (Figure 6) indicates that the carbinolamine undergoes a substantial rotation during the course of the eliminative reaction. This movement disrupts the interactions of the α-carboxylate and α-hydroxyl groups of the carbinolamine

intermediate with Lys78 and Asp118, respectively. The only interaction maintained by the α-carboxylate of the keto acid product is the electrostatic interaction with Lys66. The keto oxygen of the product is positioned such that it forms strong hydrogen bonds with the ϵ-amino group of Lys78 and the main-chain nitrogen of Gly40.

In our analysis of the first models of L-phenylalanine dehydrogenase, we attributed the inability of the enzyme to catalyze the direct reduction of phenylpyruvate to the formation of specific hydrogen bonds with key residues in the active site. Superposition of the E·NAD^+·phenylpyruvate and E·NAD^+·L-3-phenyllactate structures (Figure 6) demonstrates that the same active-site residues responsible for preventing the enzymatic reduction of phenylpyruvate, namely, Lys78 and Gly40, also prevent the enzymatic oxidation of L-3-phenyllactate. In both instances, hydrogen bonds with these residues serve to draw the α-carbon of the ligand away from the nicotinamide ring of the dinucleotide. In addition, the catalytic water molecule observed in the E·NADH·L-phenylalanine complex is not present in these complexes, because its binding site is occupied by the ligands. It is the hydrogen bond interactions of this water, along with those of Pro117 and Asp118, that position L-phenylalanine for deprotonation and subsequent hydride transfer to NAD^+. Thus, while the results of our kinetic experiments with 3-phenylpropionate and 2-phenylethylamine argue that the interactions of the α-amino group of L-phenylalanine are relatively unimportant for substrate binding, the structures of the complexes we have determined demonstrate that the interactions of this α-amino group within the active site are, indeed, necessary for catalysis. Given the structural similarity of L-phenylalanine dehydrogenase to other amino acid dehydrogenases, we expect that the interactions responsible for redox specificity and catalysis in this enzyme also govern the specificity and catalysis of many enzymes of this family.

ACKNOWLEDGMENT

The authors thank Dr. Werner Hummel at the Institut für Enzymtechnologie, Universität Düsseldorf in der KFA Jülich, D-5170 Jülich, Germany, for the initial gift of *Rhodococcus* sp. M4 and for useful discussions. The generous support of Dr. Hazel M. Holden in the structural determinations is also gratefully acknowledged. Finally, we thank Dr. W. W. Cleland for helpful suggestions and insights concerning the chemical mechanism.

REFERENCES

1. Hummel, W., Weiss, N., and Kula, M.-R. (1984) *Arch. Microbiol. 137*, 47−52.
2. Asano, Y., Nakazawa, A., and Endo, K. (1987) *J. Biol. Chem. 262*, 10346−10354.
3. de Boer, L., van Rijssel, M., Euverink, G. J., and Dijkhuizen, L. (1989) *Arch. Microbiol. 153*, 12−18.
4. Ohshima, T., Takada, H., Yoshimura, T., Esaki, N., and Soda, K. (1991) *J. Bacteriol. 173*, 3943−3948.
5. Hummel, W., Schütte, H., Schmidt, E., Wandrey, C., and Kula, M.-R. (1987) *Appl. Microbiol. Biotechnol. 26*, 409−416.
6. Ondetti, M. A., and Cushman, D. W. (1981) *J. Med. Chem. 24*, 355−361.
7. Abrams, W. B., Davies, R. O., and Ferguson, R. K. (1984) *Fed. Proc. 43*, 1314−1321.
8. Wendel, U., Koppelkam, M., Hummel, W., Sander, J., and Langenbeck, U. (1990) *Clin. Chim. Acta 192*, 165−170.
9. Wendel, U., Koppelkam, M., and Hummel, W. (1991) *Clin. Chim. Acta 201*, 95−98.
10. Wichmann, R., Wandrey, C., Bückmann, A. F., and Kula, M.-R. (1981) *Biotechnol. Bioeng. 23*, 2789−2802.
11. Vanhooke, J. L., Thoden, J. B., Brunhuber, N. M. W., Blanchard, J. S., and Holden, H. M. (1999) *Biochemistry 38*, 2326−2339.
12. Rossman, M. G., Liljas, A., Brändén, C. I., and Banaszak, L. J. (1975) *The Enzymes* 3rd ed., Vol. 11, pp 62−102.
13. Stillman, T. J., Baker, P. J., Britton, K. L., and Rice, D. W. (1993) *J. Mol. Biol. 234*, 1131−1139.
14. Baker, P. J., Turnbull, A. P., Sedelnikova, S. E., Stillman, T. J., and Rice, D. W. (1995) *Structure 3*, 693−705.
15. Scapin, G., Reddy, S. G., and Blanchard, J. S. (1996) *Biochemistry 35*, 13540−13551.
16. Orr, G. A., and Blanchard, J. S. (1984) *Anal. Biochem. 142*, 232−234.
17. Fasman, G. D., Ed. (1976) *Handbook of Biochemistry and Molecular Biology* 3rd ed., Vol. I, p 189, CRC Press, Cleveland.
18. Cleland, W. W. (1979) *Methods Enzymol. 63*, 103−138.
19. Otinowski, Z., and Minor, W. (1997) *Methods Enzymol. 276: Macromol. Crystallogr. Part A*, 307−326.
20. Tronrud, D. E., TenEyck, L. F., and Matthews, B. W. (1987) *Acta Crystallogr. A 43*, 489−501.
21. Jones, T. A. (1978) *J. Appl. Crystallogr. 11*, 268−272.
22. Roussel, A., and Cambillau, C. (1991) *Silicon Graphics Geometry Partners Directory*, p 86, Silicon Graphics, Mountain View, CA.
23. Meister, A. (1990) *Ann. N.Y. Acad. Sci. 585*, 13−31.
24. Janas, K. M. (1993) *Acta Biochim. Pol. 40*, 451−454.
25. Taylor, R. G., Levy, H. L., and McInnes, R. R. (1991) *Mol. Biol. Med. 8*, 101−116.
26. Brunhuber, N. M. W., and Blanchard, J. S. (1994) *Crit. Rev. Biochem. Mol. Biol. 29*, 415−467.
27. Baker, P. J., Sawa, Y., Shibata, H., Sedelnikova, S. E., and Rice, D. W. (1998) *Nat. Struct. Biol. 5*, 561−567.
28. Misono, H., Yonezawa, J., Nagata, S., and Nagasaki, S. (1989) *J. Bacteriol. 171*, 30−36.
29. Asano, Y., Nakazawa, A., Endo, K., Hibino, Y., Ohmori, M., Numao, N., and Kondo, K. (1987) *Eur. J. Biochem. 168*, 153−159.
30. Bradshaw, C. W., Wong, C.-H., Hummel, W., and Kula, M.-R. (1991) *Bioorg. Chem. 19*, 29−39.
31. Ohshima, T., and Soda, K. (1979) *Eur. J. Biochem. 100*, 29−39.
32. Alizade, M. A., Bressler, R., and Brendel, K. (1975) *Biochim. Biophys. Acta 397*, 5−8.
33. Hashimoto, H., Misono, H., Nagata, S., and Nagasaki, S. (1989) *Agric. Biol. Chem. 53*, 1175−1176.
34. Cleland, W. W. (1977) *Adv. Enzymol. Relat. Areas Mol. Biol. 45*, 273−387.
35. Rife, J. E. and Cleland, W. W. (1980) *Biochemistry 19*, 2328−2333.
36. Maniscalco, S. J., Saha, S. K., Vicedomine, P., and Fisher, H. F. (1996) *Biochemistry 35*, 89−94.
37. Kraulis, P. J. (1991) *J. Appl. Crystallogr. 24*, 946−950.

BI000494C